

Floquet Gauge Anomaly Inflow and Arbitrary Fractional Charge in Periodically Driven Topological-Normal Insulator Heterostructures

Yiming Pan^{1,2,3,*}, Zhaopin Chen,^{2,3,4,†} Bing Wang,⁵ and Eilon Poem³


¹*School of Physical Science and Technology and Center for Transformative Science, ShanghaiTech University, Shanghai 200031, China*

²*Physics Department and Solid-State Institute, Technion, Haifa 32000, Israel*

³*Department of Physics of Complex Systems, Weizmann Institute of Science, Rehovot 76100, Israel*

⁴*Department of Electrical Engineering Physical Electronics, Tel Aviv University, Ramat Aviv 69978, Israel*

⁵*National Laboratory of Solid State Microstructures and School of Physics, Nanjing University, Nanjing 210093, China*

 (Received 17 June 2022; revised 14 November 2022; accepted 27 February 2023; published 1 June 2023)

Usually, when coupling in a background gauge field, topological zero modes would yield an anomalous current at the interface, culminating in the zero-mode anomaly inflow, which is ultimately conserved by extra contributions from the topological bulk. However, the anomaly inflow mechanism for guiding Floquet steady states is rarely explored in periodically driven systems. Here we synthesize a driven topological-normal insulator heterostructure and propose a Floquet gauge anomaly inflow, associated with the occurrence of arbitrary fractional charge. Through our photonic modeling, we experimentally observed a Floquet gauge anomaly as the system was driven into anomalous topological phases. Prospectively, we believe our findings could pave a novel avenue on exploring Floquet gauge anomalies in driven systems of condensed matter, photonics, and ultracold atoms.

DOI: [10.1103/PhysRevLett.130.223403](https://doi.org/10.1103/PhysRevLett.130.223403)

Quantum anomaly is an anomalous current term that arises when a classical symmetry is broken at a quantum-mechanical level [1,2]. It provides a mechanism for symmetry breaking that differs from spontaneous and explicit symmetry breaking [3]. Initially, this anomalous symmetry breaking was discovered in the neutral pion decay process by Alder [4] and Bell and Jackiw [5]. Later, a large number of anomalies were revealed as pathological features of quantum field theories (QFTs) [1]. As an example, when chiral fermions interact with a background gauge field (e.g., electromagnetic field), they generate an anomalous current that breaks the corresponding gauge symmetry, namely, gauge anomalies. Since the mid 1980s, there exists a comprehensive understanding of anomalies by means of the Callan-Harvey mechanism [6–8], which demonstrates that the cancellation of the zero-mode anomalies on defects (e.g., domain walls, vortex) is achieved through an extra current inflow from the bulk [see Fig. 1(a)]. Specifically, for a quantum physical system in the low-energy limit, an anomaly must be matched since massive degrees of freedom at high energy scales are integrated out [9,10]. This anomaly matching requirement can bring many nontrivial consequences in seemingly different systems, such as zero modes in topological insulators [11,12], massless excitations in spin chains [13], and long-range entanglement in quantum matter [14,15].

Nowadays, the occurrence of anomalies has been widely verified in the development of condensed matter physics, which contributed to the discovery of the quantum Hall

effect [16–18] and symmetry-protected topological phases (SPT phases) [11,12]. For instance, SPT phases are a material manifestation of the generalized ‘t Hooft anomaly of global discrete symmetries [19], which differs from the gauge anomaly of continuous symmetries. Recent advances in understanding anomalies, including nontrivial edge states on the boundaries of SPT phases [20] elucidate the connection between anomalies and bulk-boundary correspondence in topological materials. On the other

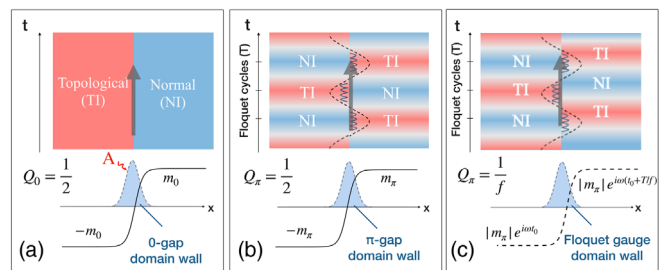


FIG. 1. Anomaly inflow on a domain wall in static and periodically driven TI/NI heterostructures. (a) The domain wall construction for zero-mode anomalies in the presence of a background gauge field A . The topological excitation holds a $1/2$ fractional charge. (b) The anomalous domain wall construction for the π -mode anomaly. The anomalous topological excitation holds a $1/2$ fractional charge. (c) A generalized Floquet-gauge-induced π -mode domain wall construction. The Floquet gauge for the two sides is relatively shifted by T/f . The fractional charge is $Q_\pi = 1/f$.

hand, SPT phases have been implemented in many periodically driven systems [21,22], referred to as “anomalous Floquet topological phases.” However, anomalies of Floquet systems are rarely investigated, due to the ambiguity in defining the gauge fields for guiding Floquet steady states [23,24]. In light of this, the present study seeks to uncover a wide range of anomalies in driven systems that can be applied to simulation platforms such as topological photonics [25].

Recent implementation of artificial gauge fields in photonic systems enables us to study the anomalous behavior of Floquet topological modes [26]. For instance, the artificial gauge field can be constructed by photonic geometry or periodic modulation [24]. Inspired by the realization of anomalous topological phases in periodically modulated photonic lattices [27–29], we recently presented a novel type of Floquet-engineered anomaly on a driven domain wall, which we dubbed the “ π -mode anomaly” (with respect to the zero mode anomaly) [27,28].

In this Letter, we find that the π -mode anomaly arises naturally when the Floquet gauge [30,31] is appropriately tuned in our setting of driven topological-normal insulator (TI/NI) heterostructures. The spatiotemporal configuration of the Floquet gauge causes anomaly inflow and fractional charges of arbitrary number. Our prediction and observation in photonic lattice unveil a new Callan-Harvey mechanism in driven systems: the π -mode anomaly at the driven interface can be matched by a newly reported gauge anomaly inflow from the Floquet bulk, which offers a new approach to drive gauge anomalies in the context of Floquet engineering of photonic materials and condensed matter.

Floquet TI/NI heterostructure.—To characterize the emergence of a driven domain wall, we construct a periodically driven TI/NI heterostructure. As shown in Fig. 1(a), a static domain wall is formed when a topological insulator interfaced with a normal insulator. The topological excitations of this static heterostructure in the presence of background gauge field (A) are well understood [7]. In contrast, as shown in Fig. 1(b), a *driven* heterostructure consists of two topologically distinct phases that periodically alternate. To specifically characterize the driven TI/NI setup, we assume that the Hamiltonian relevant to the left-hand side of the heterostructure is given by a piecewise Floquet cycle,

$$H^{(L)}(t) = \begin{cases} H_{\text{TI}}, & t \in (-\frac{T}{4}, \frac{T}{4}), \\ H_{\text{NI}}, & t \in (\frac{T}{4}, \frac{3T}{4}). \end{cases} \quad (1)$$

Likewise, the Hamiltonian of the right-hand side is $H^{(R)}(t) = H^{(L)}(t + T/2)$, where the topological invariants of the static SPT phase for the two instantaneous bulk Hamiltonians H_{TI} and H_{NI} are topologically distinct, $\nu(H_{\text{TI}}) \neq \nu(H_{\text{NI}})$. As the Atiyah-Singer index theory states that the number of zero modes at the interface equals

the difference between the topological invariants [11,12], for the static TI/NI setup we can predict that zero-mode anomaly arises when coupling to a gauge field [Fig. 1(a)]. However, for the driven scenario, we have to extend the definitions of topological invariants into periodically driven systems [21].

Take the one-dimensional driven Su-Schrieffer-Heeger (SSH) model as an example [32]. The bulk Hamiltonian with the dimerized coupling profiles is given by $H^{(L,R)}(t) = \sum_{i=1}^{N-1} [\kappa_0 + (-1)^i \delta\kappa_1 \cos(\omega t + \theta^{(L,R)})] c_i^\dagger c_{i+1} + h.c.$, where c_i^\dagger and c_i are the creation and annihilation operators at the site i , and N is the total number of lattice sites. The second off-diagonal term represents the nearest-neighbor hoppings, where κ_0 is the constant coupling strength and $\delta\kappa_1$ is the periodically dimerized staggered coupling strength, with $\omega = 2\pi/T$ the driven frequency and θ the initial phase. Notice that the sublattice symmetry of the SSH model is still preserved. To explore the quasienergy gap opening, the driven Hamiltonian is represented on a Floquet-Bloch basis. Considering periodic boundary condition, we transform the Hamiltonian $H^{(L,R)}$ into the momentum space: $H^{(L,R)}(k, t) = \{\kappa_0 - \delta\kappa_1 \cos(\omega t + \theta^{(L,R)}) + [\kappa_0 + \delta\kappa_1 \cos(\omega t + \theta^{(L,R)})] \cos(k)\} \sigma_1 + [\kappa_0 + \delta\kappa_1 \cos(\omega t + \theta^{(L,R)})] \times \sin(k) \sigma_2$, where $\sigma_1, \sigma_2, \sigma_3$ are Pauli matrices on the basis of sublattices in a driven SSH model, and k is the momentum index with the lattice constant $a = 1$.

The arbitrary choice of the initial phase θ is associated with the initial time t_0 , which is termed as Floquet gauge [30,31,33]. To satisfy the driven condition in Eq. (1), we pick the local gauge $\theta^{(L)} = 0$ for $H^{(L)}$ and $\theta^{(R)} = \pi$ for $H^{(R)}$, respectively. Especially, the choice of Floquet gauge, i.e., θ , or t_0 , determines the Floquet Hamiltonian [34,35], given by,

$$H_F[t_0] \equiv \frac{i}{T} \ln(\hat{T} e^{-i \int_{t_0}^{t_0+T} H(t') dt'}), \quad (2)$$

where $H(t) = H(t + T)$. The Floquet gauge is periodic and continuous in a Floquet cycle. Thus, the Floquet Hamiltonians of the two sides are related by, $H_F^{(L)}[t_0] = H_F^{(R)}[t_0 + T/2]$.

Adiabatic and high-frequency limits.—Before resolving the quasienergy spectrum, we examine two limits. First, in the adiabatic limit, we have the eigenvalue spectrum of the instantaneous Hamiltonian $H(t) = H^{(L)}(t) + H^{(R)}(t)$. In a cycle of T , we see an instantaneous zero-energy band. However, the zero-energy gap closes at two critical points $t = T/4$ and $3T/4$, leading to a phase transition since the staggered coupling instantly disappears. Consequently, the instantaneous Hamiltonian is forced to be metallic, and the zero-gap invariant is ill defined.

Second, in the high-frequency limit, an effective high-frequency-approximated Hamiltonian [31], $H_{\text{eff}}^{(L)} = H_{\text{eff}}^{(R)}$, can be obtained. Thus, the driven TI/NI interface vanishes and there is no domain wall. We apply the Magnus

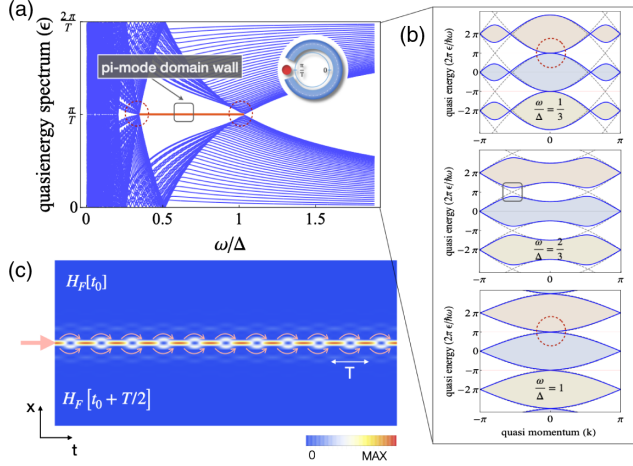


FIG. 2. The quasienergy spectrum and the π -mode eigenstate evolution from Floquet-Bloch theorem. (a) The emergence of the π -mode domain wall in the quasienergy spectrum. (b) The “open-close-open” mechanism of the topological π gap in quasi-energy-momentum space. At the driven frequencies $\omega/\Delta = 1/3, 1$, the π gap is closed nontrivially, with Δ being the bandwidth. (c) The quasienergy evolution of the π -mode eigenstate at the interface.

expansion provided by $H_{\text{eff}}^{(L,R)} = H_0 + O(1/\omega^n)$, where the zero-order term H_0 is identical to the trivial Hamiltonian without dimerization. As a result, the high-frequency approximation gives no topological protection.

Since the adiabatic and high-frequency limits are both trivial, we investigate the intermediate resonant regime. Figure 2(a) depicts the quasienergy spectrum obtained by directly solving the Floquet Hamiltonian $H_F[t_0]$ (2) (see the Supplemental Material [36], Sec. VII). From the quasienergy spectrum, we find that a π -mode eigenstate survives at a certain frequency range $(\Delta/3) < \omega < \Delta$. It indicates that instead of opening a zero gap, a π gap is opened, allowing nontrivial π -mode excitations to occur in our driven scenario.

Three spectral characteristics are worth mentioning here. (i) Using the quasienergy spectrum, we confirm that the adiabatic and high-frequency regions are topologically trivial, which is in accordance with our approximate analysis of two limits. (ii) The critical frequencies $\Delta/3$ and Δ can be explained by a level crossing between quasienergy bands. As shown in Fig. 2(b), the π gap is closed at $\omega = (\Delta/3)$ owing to the touching between the bands $n + 1$ and $n - 2$, and at $\omega = \Delta$ due to the touching between neighboring bands n and $n + 1$. (iii) The π -gap invariant ν_π is given in [37]. The gap invariants for the left- and right-handed sides are equal, $\nu_\pi(H^{(L)}) = \nu_\pi(H^{(R)}) = 1$. Because of $|\nu_\pi(H^{(L)}) - \nu_\pi(H^{(R)})| = 0$, the naïve implementation of the Atiyah-Singer theorem implies no domain walls. Surprisingly, we obtain the Floquet π -mode domain wall [Fig. 2(c)]. The Floquet domain walls in the adiabatic, intermediate, and high-frequency regimes are presented in

Fig. S8 of the Supplemental Material [36]. Also, we notice that the dynamics of the π -mode domain wall resemble the zero-mode anomaly in a quantum Hall heterostructure, see Fig. S10 [36].

Floquet gauge configuration.—To resolve the apparent contradiction, we examine the Floquet gauge in detail. Although the gap invariants of both sides are identical, the π gaps are inextricably linked to the Floquet gauge choice. The π gap can be denoted as the mass term $m_\pi^{(R)}(t_0) = m_\pi^{(L)}(t_0 + T/2)$ in the continuous limit of the driven TI/NI model, and we can find $m_\pi^{(L)}(t_0 + T/2) = -m_\pi^{(L)}(t_0)$ at $\theta = \pi$. Thus, the two bulk Hamiltonians of both sides inherit the π -gap mass terms with opposite signs. As a result, the π -mode domain wall must appear due to the nonzero index $|\nu_\pi(H^{(L)}) - [-\nu_\pi(H^{(R)})]| = 2$ [38].

To analyze this π -mode anomaly, we decompose the evolution of the driven system into two processes [35]: the *stroboscopic evolution* and the *micromotion*. The evolution operator is thus decomposed as $U(t, t_0) = V(t, t_0)e^{-iH_F[t_0](t-t_0)}$, where the periodized evolution operator $V(t, t_0) \equiv U(t, t_0)e^{iH_F[t_0](t-t_0)}$ contains the short time-scale information in a cycle related to the Floquet gauge. Now we define a gauge-independent Floquet Hamiltonian,

$$H_F[t_0] = V^{-1}(t, t_0)H_F V(t, t_0), \quad (3)$$

where the Hamiltonian $H_F = H(t) - i\partial t$ is gauge-free. The periodized evolution operator specifies an initial value of t_0 that connects to the micromotion, acting as a gauge field attached to the stroboscopic steady-state dynamics. To be specific, we propose a local spatiotemporal configuration on the choice of initial time: $t_0 = t_0(x, t)$. Here, $t_0(x, t)$ is the Floquet gauge field that can guide steady states in a slowly varying way compared to the drive.

Floquet-gauge-induced current.—To evaluate the appearance of the Floquet gauge anomaly, we use the $k\rho$ approximation to calculate the Floquet Hamiltonian by truncating the Floquet state-space into two Floquet bands, n and $n + 1$ [see the middle subfigure in Fig. 2(b)],

$$H_{\text{FD}}^{(\pi)}[t_0] = \frac{\omega}{2}I_2 \pm \sqrt{1 - \left(\frac{\omega}{\Delta}\right)^2} \begin{pmatrix} \kappa_0 p & -ie^{i\omega t_0} \delta\kappa_1 \\ ie^{-i\omega t_0} \delta\kappa_1 & -\kappa_0 p \end{pmatrix}, \quad (4)$$

where $p = k \pm \cos^{-1}(\omega/\Delta)$ and $\Delta = 4\kappa_0$. The local Floquet gauges for both sides can be rephrased as $\theta^{(L)} = \omega t_0$ ($x < 0$), $\theta^{(R)} = \omega(t_0 + T/2)$ ($x > 0$). The corresponding Floquet-Dirac Hamiltonian is given by $H_{\text{FD}}^{(\pi)} = V(t_0)H_{\text{FD}}^{(\pi)}[t_0]V^{-1}(t_0) = (\omega/2)I_2 \pm \sqrt{1 - (\omega/\Delta)^2}(\kappa_0 p\sigma_3 + \delta\kappa_1\sigma_2)$, with $V(t_0) = e^{-i\omega t_0\sigma_3/2}$. The π -gap mass term $m_\pi = \sqrt{1 - (\omega/\Delta)^2}\delta\kappa_1\sigma_2$ is then gauge independent.

By applying (3) to the mass terms of both sides, we can obtain

$$m_{\pi}^{(L)} = V^{-1}(t_0)m_{\pi}V(t_0) = -m_{\pi}^{(R)}, \quad (5)$$

with $m_{\pi}^{(L,R)} = \pm\sqrt{1 - (\omega/\Delta)^2}\delta\kappa_1\sigma_2$. Consequently, it reveals that the left-handed and the right-handed mass terms have opposite signs, suggesting the appearance of a gauge anomaly on the driven interface [7,38]. Alternatively, to demonstrate the anomaly associated with the local Floquet gauge $t_0(x, t)$ [Fig. 2(c)], we apply the Goldstone-Wilczek approach [8] to determine the current of Floquet-Dirac Hamiltonian [Eq. (4)]

$$\langle j^{\mu} \rangle = \frac{1}{2\pi} \epsilon^{\mu\nu} \partial_{\nu} [\omega t_0(x, t)], \quad (6)$$

with the notations $\mu, \nu = 0, 1$, $\epsilon^{\mu\nu}$ is an antisymmetry tensor, where $\epsilon^{01} = 1$ in $1 + 1$ spacetime.

Fractional charge.—For our setup in Fig. 1(b), the total quantum number is

$$Q_{\pi} = \frac{\omega}{2\pi} \int \partial_x t_0(x) dx = \frac{\omega}{2\pi} [t_0(+\infty) - t_0(-\infty)] = \frac{1}{2}. \quad (7)$$

The resulting fractional quantum number $Q_{\pi} = 1/2$ is similar to the fractional charge proposed by Jackiw and Rebbi [8,16,32,39]. Moreover, the driven fractional charge can be arbitrary, $Q_{\pi} = 1/f$, as the Floquet gauge of both sides can be relatively twisted by $t_0 \rightarrow t_0 + (T/f)$, as shown in Fig. 1(c). We note that the formation of arbitrary fractional charges can be demonstrated by driving a local domain wall with a configuration of Floquet gauge field. However, the physics of fractional charge is elusive because one cannot directly detect the fractional charge by local excitation due to its *global* topological nature.

Figure 3 depicts the confinement of driven domain walls with respect to different fractional charges. When the fractional charge ($1/f$) decreases, the confinement weakens, indicating that the topological protection becomes more fragile. Thus, a smaller fractional charge is more difficult to excite. The driven TI/Ni setup demonstrates that the period drive may readily create arbitrary fractional charges, which may be interesting for exploration in simulation platforms such as cold atoms.

Floquet gauge anomaly inflow.—Assuming that the Floquet gauge varies both spatially and temporally, the Goldstone-Wilczek charge and current densities are [Eq. (6)],

$$\rho_{\pi} = \frac{1}{2\pi} \partial_x [\omega t_0(x, t)]; \quad \vec{j}_{\pi} = -\frac{1}{2\pi} \partial_t [\omega t_0(x, t)]. \quad (8)$$

The fractional charge density (ρ_{π}) is mainly pinned on the interface due to the spatial kink configuration, while the

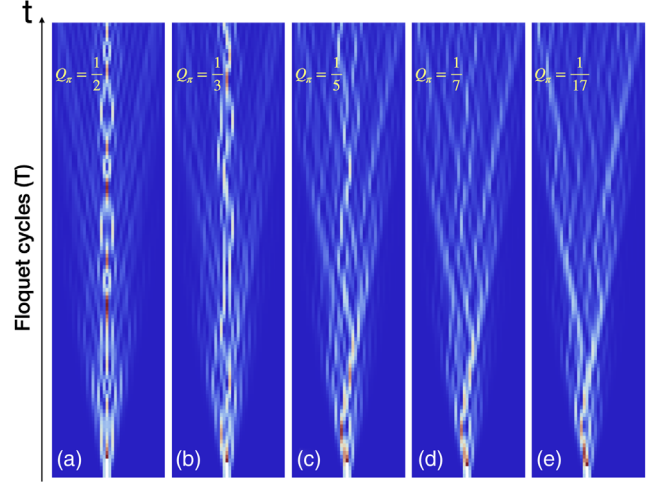


FIG. 3. The confinement signature of Floquet gauge anomaly with arbitrary fractional charges in driven systems. (a)–(e) Time evolutions with fractional charge of $Q_{\pi} = 1/2, 1/3, 1/5, 1/7,$ and $1/17$, respectively, are presented, respectively, from left to right. The fractional charge is topologically induced by the spatial change of the Floquet gauge. Topological excitations with smaller charges are more weakly confined.

nonzero current (\vec{j}_{π}) is distributed in the topological bulk that corresponds to a topological pumping effect [40,41]. As a result, the anomalous current is conserved,

$$\partial_{\mu} \langle j^{\mu} \rangle = \frac{\partial \rho_{\pi}}{\partial t} + \nabla \cdot \vec{j}_{\pi} = 0. \quad (9)$$

We observe that the domain-wall dynamics with fractional charge match an anomalous current flow towards the interface. *This is the predicted Floquet gauge anomaly in a periodically driven system*, inspired by the Callan-Harvey mechanism from quantum fields [7].

Experimental verification.—To experimentally observe the π -mode anomaly, we construct an optical analog of a driven TI/Ni heterostructure using femtosecond laser direct waveguide writing [42]. Via the quantum-optical analogy [25], the electron wave function in time (t) is mimicked by light propagation along the direction (z). The fabrication and setup are given in the Supplemental Material [36] (Sec. I and Figs. S1, S2, and S3).

Figure 4 demonstrates our prediction and measurement results for the adiabatic, intermediate, and high-frequency regimes. For each regime, we measure the light intensity distribution at the output of the corresponding waveguide structure. As seen in Figs. 4(c), 4(f), and 4(i), only the structure corresponding to the intermediate drive regime (curving period $T = 8.3$ mm) displays an output intensity distribution confined to the central waveguide of the array. The output intensity distributions of the other structures exhibit diffusive behavior, both in the adiabatic regime [$T = 50$ mm, see Figs. 4(b), 4(e), and 4(h)] and in the high-frequency regime ($T = 2.5$ mm, see Figs. 4(d), 4(g),

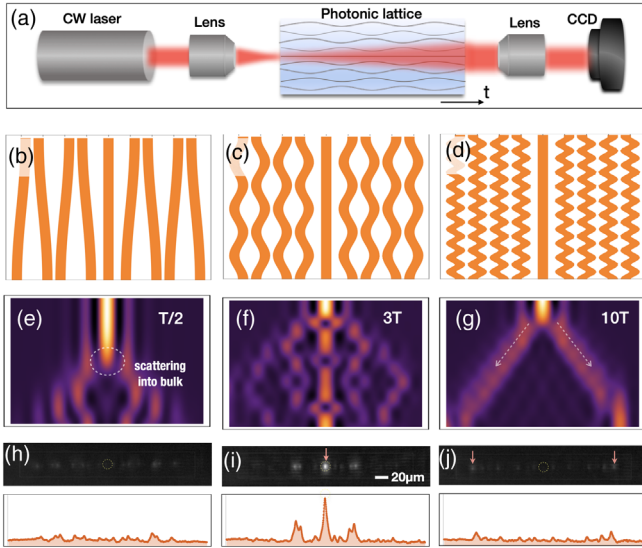


FIG. 4. Experimental observation of the Floquet π -mode anomaly ranging from the adiabatic limit to the high-frequency limit. (a) The reading system for detecting the output intensity distribution of the photonic modeling of driven TI/Ni heterostructures. The designed structures (b)–(d), simulated propagation dynamics (e)–(g), and experimental measurements of the output intensity distributions (h)–(j) are shown. The π -mode anomaly appears only at the intermediate frequency range (c),(f),(i).

and 4(j)]. This observed behavior agrees well with the calculated quasienergy spectrum [Fig. 2(a)]. As a calibration, we also fabricated a straight waveguide array and observed the zero-mode domain walls, see the Supplemental Material [36], Secs. 3 and 4, Figs. S4–S7.

We would like to note to important points regarding the characteristics of our setup. First, our experiment is based on photonic modeling by translating the time into the propagation direction. Keeping this in mind, our measurement is an analog of the anomaly dynamics of the π -mode domain walls, allowing us to measure the evolution. However, to further detect the micromotion with an arbitrary Floquet gauge, an optical near-field measurement [27] is required to record the field distribution, which is beyond the current capabilities of our optical system.

Second, fractional charges cannot be directly seen in the waveguide array platform at hand. One reason for that is that fractional charge is a nonlocal excitation induced by a global topological structure [43]. A second reason is that our photonic platform is a classical system, and all bosonic particles might occupy the same state, preventing the detection of fractional excitation at a quantum level. In light of the global phase structure of fractional excitations [Eq. (7)], we would suggest identifying the optical spectral feature of fractional charges by using optical spectroscopy and interferometry. A recent work observed a signature of fractional charges in photonic crystals by detecting an abrupt change in the local optical density of states [44]. Nevertheless, direct detection and manipulation of

fractional charges in optical and photonic systems, or even in condensed matter experiments [45–47], remains a long-standing open issue.

Conclusion.—We showed that a driven topological-normal insulator heterostructure can create Floquet gauge anomaly inflow and excitations with an arbitrary fractional charge. For that purpose, we proposed a Floquet-engineered Callan-Harvey mechanism. Using femtosecond laser direct writing, we further experimentally observed the confinement of a π -mode anomaly in periodically modulated photonic lattices. Still, many issues pertinent to Floquet gauge anomalies, including the coexistence of zero and π -mode anomalies, and direct detection of fractional charges, remain unexplored. We anticipate our work will stir the curiosity of researchers from several fields, such as condensed matter, cold atoms, and even quantum fields, and prompt them to study periodically driven systems.

The authors would like to thank Yehonatan Gilead, Uri Levy, Xinbin Song, and Nir Davidson for the stimulating discussions and their useful comments. In particular, we would like to thank the late professor Yaron Silberberg for his inspiration and contribution to the early stages of this work. The work was supported in parts by DIP (German-Israeli Project Cooperation) No. 04340302000, ISF (Israel Science Foundation) No. 00010001000, and by ICORE—Israel Center of Research Excellence program of the ISF, and by the Crown Photonics Center. Z. C. acknowledges a fellowship provided by the Helen Diller quantum center at the Technion (Haifa, Israel).

Appendix: Floquet gauge anomaly inflow from the kp approximation quasienergy spectrum.—To assess the Floquet gauge anomaly in our setup, we build an effective Dirac-type Hamiltonian and then use the Goldstone-Wilczek formula to account for the Floquet quasienergy states. The Floquet-Dirac Hamiltonian can be derived from the Hamiltonian we constructed in a Floquet TI/Ni heterostructure, which is given by

$$\begin{aligned}
 H(k, t) = & \{ \kappa_0 - \delta\kappa_1 \cos(\omega t + \theta) \\
 & + [\kappa_0 + \delta\kappa_1 \cos(\omega t + \theta)] \cos(k) \} \sigma_1 \\
 & + [\kappa_0 + \delta\kappa_1 \cos(\omega t + \theta)] \sin(k) \sigma_2, \quad (A1)
 \end{aligned}$$

where σ_1, σ_2 are Pauli matrices on the basis of sublattices, and k is the momentum index. For a general spatiotemporal varying Floquet gauge $t_0(x, t)$, the phase is given by $\theta = \omega t_0(x, t)$. For our concern, the gauge is only spatially dependent, i.e., $\theta^{(L)} = \omega t_0(x < 0)$, $\theta^{(R)} = \omega(t_0 + T/2) \times (x > 0)$. The spatial dependency of the Floquet gauge $t_0(x, t)$ results in a fractional charge, and its temporal dependence results in an anomalous current (i.e., Floquet topological pumping) as shown in the following derivation. The spatiotemporal variation of $t_0(x, t)$ would then activate

the Floquet anomaly inflow mechanism, allowing the conversation between the transferred fractional charge and the accumulated anomalous current.

Considering the time periodicity in $H(k, t)$, we can define the Floquet Hamiltonian H_F in terms of the photon band replica

$$H_F = \begin{pmatrix} \ddots & \vdots & \vdots & \vdots & \vdots & \vdots & \ddots \\ \dots & H^{(0)} - 2\omega & H^{(-1)} & 0 & 0 & 0 & \dots \\ \dots & H^{(1)} & H^{(0)} - \omega & H^{(-1)} & 0 & 0 & \dots \\ \dots & 0 & H^{(1)} & \boxed{H^{(0)}} & \boxed{H^{(-1)}} & 0 & \dots \\ \dots & 0 & 0 & \boxed{H^{(1)}} & \boxed{H^{(0)} + \omega} & H^{(-1)} & \dots \\ \dots & 0 & 0 & 0 & H^{(1)} & H^{(0)} + 2\omega & \dots \\ \ddots & \vdots & \vdots & \vdots & \vdots & \vdots & \ddots \end{pmatrix} \quad (\text{A2})$$

where the matrix block $H^{(n)}$ represents the n th order Fourier component of $H(k, t)$. The leading three terms are given by

$$\begin{aligned} H^{(0)} &= [(\kappa_0 - \delta\kappa_0) + (\kappa_0 + \delta\kappa_0)\cos(k)]\sigma_x \\ &\quad + [(\kappa_0 + \delta\kappa_0)\sin(k)]\sigma_y, \\ H^{(1)} &= \left[-\frac{\delta\kappa_1 e^{i\theta}}{2} + \frac{\delta\kappa_1 e^{i\theta}}{2}\cos(k) \right] \sigma_x + \frac{\delta\kappa_1 e^{i\theta}}{2}\sin(k)\sigma_y, \\ H^{(-1)} &= \left[-\frac{\delta\kappa_1 e^{-i\theta}}{2} + \frac{\delta\kappa_1 e^{-i\theta}}{2}\cos(k) \right] \sigma_x + \frac{\delta\kappa_1 e^{-i\theta}}{2}\sin(k)\sigma_y, \end{aligned} \quad (\text{A3})$$

with $H^{(\pm n)}(k) = 0$ for $n \geq 2$. In this case, the diagonal terms, $n = 0, \pm 1, \dots$ are the artificial photon replica with discrete energy $n\omega$ and the decoupled local electron energy $H^{(0)}$. The secondary-diagonal terms $H^{(\pm 1)}$ represent the artificial photon scattering between two neighbor photon

bands n and $n + 1$, where the sign “−” denotes the emission process and the sign “+” denotes the absorption process. Figure 2(b) depicts the quasienergy spectrum H_F . At the condition $1 < \omega/\Delta < 1/3$, two neighboring bands cross and open a π gap, forming a local Dirac Hamiltonian of Floquet quasienergy bands. We further apply the k_p approximation at the crossing points with the momentum $k_{\pm} = \pm \cos^{-1}(\omega/\Delta)$ to eliminate the other irrelevant bands, reducing the full Hamiltonian H_F into an effective Hamiltonian with a 2×2 matrix form:

$$H_{\text{FD}}^{(\pi)} = \frac{\omega}{2} I_2 \pm \sqrt{1 - \left(\frac{\omega}{\Delta}\right)^2} (\kappa_0 p \sigma_3 + \delta\kappa_1 e^{-i\theta\sigma_3} \sigma_2), \quad (\text{A4})$$

where $p = k \pm \cos^{-1}(\omega/\Delta)$ and $\Delta = 4\kappa_0$. To apply the Goldstone-Wilczek formula, we rewrite the effective Dirac Hamiltonian $H_{\text{FD}}^{(\pi)}$ in the field-quantization formulation,

$$\begin{aligned} H_{\text{FD}}^{(\pi)} &= \int dx \psi^\dagger(x) \left(\frac{\omega}{2} I_2 \pm \sqrt{1 - \left(\frac{\omega}{\Delta}\right)^2} \right. \\ &\quad \left. \times (\kappa_0 p \sigma_3 + \delta\kappa_1 e^{-i\theta(x,t)\sigma_3} \sigma_2) \right) \psi(x). \end{aligned} \quad (\text{A5})$$

Here, the field $\psi(x)$ represents the quantized steady state on the Floquet band. It should be mentioned that the field $\psi(x)$ is actually bosonic in our photonic setup. Since the anti-commutation relation obeys $\{H(k, t), \sigma_3\} = 0$, our Floquet TI/NI heterostructure should have a chiral (sub-lattice) symmetry specified by the Pauli operator σ_3 . However, when we perform a chiral gauge transformation $\psi(x) \rightarrow e^{i\theta(x,t)\sigma_3/2}\psi(x)$, we obtain the following Hamiltonian with an additional potential term:

$$\begin{aligned} &e^{i\theta(x,t)\sigma_3/2} \left\{ \frac{\omega}{2} I_2 \pm \sqrt{1 - \left(\frac{\omega}{\Delta}\right)^2} (\kappa_0 p \sigma_3 + \delta\kappa_1 e^{-i\theta(x,t)\sigma_3} \sigma_2) \right\} e^{-i\theta(x,t)\sigma_3/2} \\ &\rightarrow \frac{\omega}{2} I_2 \pm \sqrt{1 - \left(\frac{\omega}{\Delta}\right)^2} \{ \kappa_0 p \sigma_3 + \delta\kappa_1 e^{-i\theta(x,t)\sigma_3} \sigma_2 - \kappa_0 \partial_x [\theta(x, t)] \}, \end{aligned}$$

where we use the momentum operator $p \rightarrow -i\partial_x$ in real space. The last term suggests that a spatially varying Floquet gauge would add a potential corresponding to the rate of spatial variation in $\theta(x, t)$. Since we obtained the prototypical Jackiw-Rebbi model with the Dirac-type Hamiltonian $H_{\text{FD}}^{(\pi)}$ [Eq. (A5)], there are several approaches to obtaining the Floquet gauge anomaly and Jackiw-Rebbi domain wall solutions [41], similar to the treatment of zero-mode domain wall and zero-mode anomaly (see the Supplemental Material [36]). Without losing the generality, we can directly apply the Goldstone-Wilczek formula [8]

for the positive branch at k_+ , to obtain the anomalous 2-form current term [see Eq. (6) in the main text], given by

$$\langle j^\mu \rangle = \frac{1}{2\pi} \epsilon^{\mu\nu} \partial_\nu [\omega t_0(x, t)], \quad (\text{A6})$$

As a result, the fractional charge density and anomalous current density are obtained as

$$\rho_\pi(x, t) = \frac{\omega}{2\pi} \partial_x t_0(x, t), \quad \vec{j}_\pi(x, t) = -\frac{\omega}{2\pi} \partial_t t_0(x, t). \quad (\text{A7})$$

It implies that the fractional charge originates from the spatial variation of the Floquet gauge $t_0(x, t)$ while the anomalous current originates from the temporal variation. Finally, when the gauge field $t_0(x, t)$ is spatiotemporally variable [see Eq. (9) in the main text], there is a nontrivial conservation between fractional charge and anomalous current, satisfying equation (9).

*Corresponding author.

yiming.pan@shanghaitech.edu.cn

†Corresponding author.

zhaopin.chen@campus.technion.ac.il

- [1] K. Fujikawa and H. Suzuki, *Path Integrals and Quantum Anomalies* (Clarendon, Oxford, 2004).
- [2] R. A. Bertlmann, *Anomalies in Quantum Field Theory* (Oxford University Press, New York, 2000), Vol. 91.
- [3] E. Castellani and R. Dardashti, Symmetry breaking, in *The Routledge Companion to Philosophy of Physics* (Routledge, Abingdon, 2021), pp. 620–631.
- [4] S. L. Adler, Axial-vector vertex in spinor electrodynamics, *Phys. Rev.* **177**, 2426 (1969).
- [5] J. S. Bell and R. Jackiw, A PCAC puzzle: $\Pi^0 \rightarrow \gamma\gamma$ in the σ -model, *Il Nuovo Cimento A (1965–1970)* **60**, 47 (1969).
- [6] H. B. Nielsen and M. Ninomiya, The Adler-Bell-Jackiw anomaly and Weyl fermions in a crystal, *Phys. Lett.* **130B**, 389 (1983).
- [7] C. G. Callan, Jr and J. A. Harvey, Anomalies and fermion zero modes on strings and domain walls, *Nucl. Phys.* **B250**, 427 (1985).
- [8] J. Goldstone and F. Wilczek, Fractional Quantum Numbers on Solitons, *Phys. Rev. Lett.* **47**, 986 (1981).
- [9] G. 't Hooft, Symmetry Breaking through Bell-Jackiw Anomalies, *Phys. Rev. Lett.* **37**, 8 (1976).
- [10] G. Hooft, *Naturalness, Chiral Symmetry, and Spontaneous Chiral Symmetry Breaking*, in *Recent Developments in Gauge Theories* (Springer, New York, 1980), pp. 135–157.
- [11] M. Z. Hasan and C. L. Kane, Colloquium: Topological insulators, *Rev. Mod. Phys.* **82**, 3045 (2010).
- [12] X.-L. Qi and S.-C. Zhang, Topological insulators and superconductors, *Rev. Mod. Phys.* **83**, 1057 (2011).
- [13] T. Sulejmanpasic and Y. Tanizaki, $C - P - T$ anomaly matching in bosonic quantum field theory and spin chains, *Phys. Rev. B* **97**, 144201 (2018).
- [14] X.-G. Wen, Topological order: From long-range entangled quantum matter to a unified origin of light and electrons, *Int. Scholarly Res. Not.* **2013** (2013).
- [15] X.-G. Wen, Classifying gauge anomalies through symmetry-protected trivial orders and classifying gravitational anomalies through topological orders, *Phys. Rev. D* **88**, 045013 (2013).
- [16] A. J. Niemi and G. W. Semenoff, Axial-Anomaly-Induced Fermion Fractionization and Effective Gauge-Theory Actions in Odd-Dimensional Space-Times, *Phys. Rev. Lett.* **51**, 2077 (1983).
- [17] D. Tong, Lectures on the quantum Hall effect, [arXiv: 1606.06687](https://arxiv.org/abs/1606.06687).
- [18] K. v Klitzing, G. Dorda, and M. Pepper, New Method for High-Accuracy Determination of the Fine-Structure Constant Based on Quantized Hall Resistance, *Phys. Rev. Lett.* **45**, 494 (1980).
- [19] E. Witten, Fermion path integrals and topological phases, *Rev. Mod. Phys.* **88**, 035001 (2016).
- [20] D. Tong, *Gauge Theory*, Lecture Notes (DAMTP, Cambridge, 2018).
- [21] M. S. Rudner, N. H. Lindner, E. Berg, and M. Levin, Anomalous Edge States and the Bulk-Edge Correspondence for Periodically Driven Two-Dimensional Systems, *Phys. Rev. X* **3**, 031005 (2013).
- [22] M. C. Rechtsman, J. M. Zeuner, Y. Plotnik, Y. Lumer, D. Podolsky, F. Dreisow, S. Nolte, M. Segev, and A. Szameit, Photonic Floquet topological insulators, *Nature (London)* **496**, 196 (2013).
- [23] L. Yuan, Y. Shi, and S. Fan, Photonic gauge potential in a system with a synthetic frequency dimension, *Opt. Lett.* **41**, 741 (2016).
- [24] Y. Lumer, M. A. Bandres, M. Heinrich, L. J. Maczewsky, H. Herzig-Sheinfux, A. Szameit, and M. Segev, Light guiding by artificial gauge fields, *Nat. Photonics* **13**, 339 (2019).
- [25] T. Ozawa, H. M. Price, A. Amo, N. Goldman, M. Hafezi, L. Lu, M. C. Rechtsman, D. Schuster, J. Simon, and O. Zilberberg, Topological photonics, *Rev. Mod. Phys.* **91**, 015006 (2019).
- [26] M. Aidelsburger, S. Nascimbene, and N. Goldman, Artificial gauge fields in materials and engineered systems, *C.R. Phys.* **19**, 394 (2018).
- [27] Q. Cheng, Y. Pan, H. Wang, C. Zhang, D. Yu, A. Gover, H. Zhang, T. Li, L. Zhou, and S. Zhu, Observation of Anomalous π Modes in Photonic Floquet Engineering, *Phys. Rev. Lett.* **122**, 173901 (2019).
- [28] O. Zilberberg, S. Huang, J. Guglielmon, M. Wang, K. P. Chen, Y. E. Kraus, and M. C. Rechtsman, Photonic topological boundary pumping as a probe of 4D quantum Hall physics, *Nature (London)* **553**, 59 (2018).
- [29] W. Song, Y. Chen, H. Li, S. Gao, S. Wu, C. Chen, S. Zhu, and T. Li, Gauge-induced Floquet topological states in photonic waveguides, *Laser Photonics Rev.* **15**, 2000584 (2021).
- [30] M. Bukov, L. D'Alessio, and A. Polkovnikov, Universal high-frequency behavior of periodically driven systems: From dynamical stabilization to Floquet engineering, *Adv. Phys.* **64**, 139 (2015).
- [31] A. Eckardt and E. Anisimovas, High-frequency approximation for periodically driven quantum systems from a Floquet-space perspective, *New J. Phys.* **17**, 093039 (2015).
- [32] W. Su, J. R. Schrieffer, and A. J. Heeger, Solitons in Polyacetylene, *Phys. Rev. Lett.* **42**, 1698 (1979).
- [33] M. Fruchart, Complex classes of periodically driven topological lattice systems, *Phys. Rev. B* **93**, 115429 (2016).
- [34] S. Rahav, I. Gilary, and S. Fishman, Effective Hamiltonians for periodically driven systems, *Phys. Rev. A (Coll Park)* **68**, 013820 (2003).
- [35] N. Goldman and J. Dalibard, Periodically Driven Quantum Systems: Effective Hamiltonians and Engineered Gauge Fields, *Phys. Rev. X* **4**, 031027 (2014).
- [36] See Supplemental Material at <http://link.aps.org/supplemental/10.1103/PhysRevLett.130.223403> for details

- of experimental setup, sample fabrication and theoretical calculations of zero-mode and π -mode anomalies.
- [37] V. Dal Lago, M. Atala, and L.E.F.F. Torres, Floquet topological transitions in a driven one-dimensional topological insulator, *Phys. Rev. A (Coll Park)* **92**, 023624 (2015).
- [38] I. Hason, Z. Komargodski, and R. Thorngren, Anomaly matching in the symmetry broken phase: Domain Walls, CPT, and the Smith isomorphism, *SciPost Phys.* **8**, 062 (2020).
- [39] R. Jackiw and C. Rebbi, Solitons with fermion number $\frac{1}{2}$, *Phys. Rev. D* **13**, 3398 (1976).
- [40] P. Kotetes, *Topological Insulators* (Morgan & Claypool, San Rafael, 2019).
- [41] Y. T. Katan and D. Podolsky, Modulated Floquet Topological Insulators, *Phys. Rev. Lett.* **110**, 016802 (2013).
- [42] Y. Gilead, M. Verbin, and Y. Silberberg, Ensemble-Averaged Quantum Correlations between Path-Entangled Photons Undergoing Anderson Localization, *Phys. Rev. Lett.* **115**, 133602 (2015).
- [43] F. Wilczek, Some basic aspects of fractional quantum numbers, [arXiv:Cond-Mat/0206122](https://arxiv.org/abs/cond-mat/0206122).
- [44] Y. Liu, S. Leung, F.-F. Li, Z.-K. Lin, X. Tao, Y. Poo, and J.-H. Jiang, Bulk–disclination correspondence in topological crystalline insulators, *Nature (London)* **589**, 381 (2021).
- [45] V.J. Goldman and B. Su, Resonant tunneling in the quantum Hall regime: Measurement of fractional charge, *Science* (1979) **267**, 1010 (1995).
- [46] R. De-Picciotto, M. Reznikov, M. Heiblum, V. Umansky, G. Bunin, and D. Mahalu, Direct observation of a fractional charge, *Physica B Condens. Matter* **249**, 395 (1998).
- [47] J. W. Park, E. Do, J. S. Shin, S. K. Song, O. Stetsovych, P. Jelinek, and H. W. Yeom, Creation and annihilation of mobile fractional solitons in atomic chains, *Nat. Nanotechnol.* **17**, 244 (2022).